

Spectral Approach to the Relativistic Inverse Stellar Structure Problem II

Lee Lindblom and Nathaniel M. Indik

Theoretical Astrophysics 350-17, California Institute of Technology, Pasadena, CA 91125

(Dated: September 17, 2018)

The inverse stellar structure problem determines the equation of state of the matter in stars from a knowledge of their macroscopic observables (e.g. their masses and radii). This problem was solved in a previous paper by constructing a spectral representation of the equation of state whose stellar models match a prescribed set of macroscopic observables. This paper improves and extends that work in two significant ways: i) The method is made more robust by accounting for an unexpected feature of the enthalpy based representations of the equations of state used in this work. After making the appropriate modifications, accurate initial guesses for the spectral parameters are no longer needed so Monte-Carlo techniques can now be used to ensure the best fit to the observables. ii) The method is extended here to use masses and tidal deformabilities (which will be measured by gravitational wave observations of neutron-star mergers) as the macroscopic observables instead of masses and radii. The accuracy and reliability of this extended and more robust spectral method is evaluated in this paper using mock data for observables from stars based on 34 different theoretical models of the high density neutron-star equation of state. In qualitative agreement with earlier work, these tests suggest the high density part of the neutron-star equation of state could be determined at the few-percent accuracy level using high quality measurements of the masses and radii (or masses and tidal deformabilities) of just two or three neutron stars.

PACS numbers: 04.40.Dg, 97.60.Jd, 26.60.Kp, 26.60.Dd

I. INTRODUCTION

The purpose of this paper is to improve and extend the spectral approach to solving the relativistic inverse stellar structure problem developed in our earlier paper, Lindblom and Indik [1]. In that approach the density ϵ and pressure p of the matter in a particular class of stars (e.g. neutron stars) are represented as faithful parametric expressions of the form: $\epsilon(h, \gamma_k)$ and $p(h, \gamma_k)$, where h is the enthalpy of the material, and γ_k are parameters that specify the particular equation of state. Faithful in this context means that any physical equation of state has such a representation while every choice of γ_k represents a physically possible equation of state (cf. Lindblom [2]). Given a specific equation of state in this form, it is straightforward to solve the relativistic stellar structure equations to construct stellar models and their macroscopic observables, e.g. their masses $M(h_c, \gamma_k)$ and radii $R(h_c, \gamma_k)$. These macroscopic observables depend on the equation of state through the parameters γ_k , as well as the central enthalpy h_c (or equivalently the central pressure or density) of the particular stellar model. Our approach to the inverse stellar structure problem [1] determines the equation of state by adjusting the parameters γ_k (and h_c^i) in the model observables, e.g. $M(h_c^i, \gamma_k)$ and $R(h_c^i, \gamma_k)$, to match a set of prescribed values of those observables, e.g. M_i and R_i .

The spectral approach to the relativistic inverse stellar structure problem (summarized above) was tested in our first paper, Lindblom and Indik [1], using mock observational data, M_i and R_i , constructed from 34 different theoretical models of the highest density part of the neutron-star equation of state. Sequences of approximate solutions to this problem were constructed by de-

termining the spectral parameters γ_k that minimize the quantity χ^2 defined by,

$$\chi^2(\gamma_k, h_c^i) = \frac{1}{N_{\text{stars}}} \sum_{i=1}^{N_{\text{stars}}} \left\{ \left[\log \left(\frac{M(h_c^i, \gamma_k)}{M_i} \right) \right]^2 + \left[\log \left(\frac{R(h_c^i, \gamma_k)}{R_i} \right) \right]^2 \right\}. \quad (1)$$

The accuracies of the resulting spectral equations of state were then evaluated by comparing with the exact equations of state. Those tests showed that the spectral equations of state provide good approximate solutions to the relativistic inverse stellar structure problem, with (average) error levels of just a few percent using (mock) observational data from only two or three stars. These tests also showed that the accuracy of the approximations got better (on average) when more data were used and more spectral parameters were fixed by the data.

Unfortunately, our implementation of the spectral approach described above had a serious flaw. The method worked very well if the search for the minimum of $\chi^2(\gamma_k, h_c^i)$ in Eq. (1) began with a reasonably accurate initial estimate for the spectral parameters γ_k . Without an accurate initial guess, however, the code used to solve this non-linear least squares problem often crashed. This flaw made it impossible to perform searches for the true global minimum of $\chi^2(\gamma_k, h_c^i)$, or to investigate the structure of that minimum (in γ_k parameter space). One of the main objectives of this paper is to understand the cause of this problem, and to use this understanding to develop a more robust implementation of the spectral approach. The root problem turned out to be a subtle and unexpected feature of the enthalpy based representations of the equations of state. This feature is described in

some detail in Sec. II, along with the changes in our initial implementation of the spectral approach to the inverse stellar structure problem needed to accommodate it. Using the resulting more robust approach, Sec. II contains a more thorough and systematic study of the mathematical convergence of the sequence of approximate spectral equations of state produced by this method.

Our analysis of the relativistic inverse stellar structure problem up to this point has assumed that the masses and radii of neutron stars would be the first observables measured accurately. This may turn out to be the case, but the spectral approach for solving this problem does not (in principle) depend very strongly on exactly which observables are used. Recent work [3–14] has shown that gravitational-wave observations of binary neutron-star mergers should provide accurate measurements of the masses and tidal deformabilities of neutron stars once the advanced LIGO-VIRGO network of detectors becomes operational (within the next few years). The possibility of using this type of observational data to solve the inverse stellar structure problem is explored in Sec. III of this paper. A new and more efficient method for evaluating the tidal deformabilities $\Lambda(h_c, \gamma_k)$ of neutron-star models is presented in Appendix C, along with an efficient method for evaluating its derivatives with respect to the parameters h_c and γ_k . The inverse stellar structure problem is tested in Sec. III with masses and tidal deformabilities computed from the same catalog of 34 theoretical neutron-star equations of state used in our previous studies. These tests show that the high density part of the neutron-star equation of state could be determined using precision measurements of the masses and tidal deformabilities of just two or three neutron stars at about the same level of accuracy that could be achieved using mass and radius data.

Our analysis of the relativistic inverse stellar structure problem (begun in our first paper [1] and continued here) focuses on understanding some of the fundamental mathematical aspects of this problem. Is it possible to determine the neutron-star equation of state exactly from a complete exact knowledge of the macroscopic observable properties of these stars, i.e., does this problem have a unique solution? Can numerical methods can be devised whose approximate solutions converge to the exact equation of state when a complete exact knowledge of the macroscopic observables of these stars is available? What level of numerical approximation and how many macroscopic observable data points are needed to achieve reasonable levels of accuracy for “realistic” neutron-star equations of state? A number of researchers have studied various observational and data-analysis questions associated with the inverse stellar structure problem, both in the context of using mass and radius observations [15–19], and in the context of using mass and tidal deformability measurements from gravitational-wave observations [3–14]. To our knowledge, our studies of the more fundamental questions about solving the inverse stellar structure problem described in our papers are unique. We discuss

in more detail some of the basic differences between our results and those reported by others in Sec. IV.

II. IMPROVING THE METHOD

The spectral approach to the relativistic inverse stellar structure problem outlined above requires the use of a faithful parametric representation of the equation of state. There are a variety of ways to construct such representations (cf. Lindblom [2]), but the most useful for solving the relativistic stellar structure problem (and its inverse) represent the energy density ϵ and pressure p of the stellar matter as functions of the relativistic enthalpy: $\epsilon(h, \gamma_k)$ and $p(h, \gamma_k)$. The parameters γ_k specify the particular equation of state, and the relativistic specific enthalpy h is defined by the integral,

$$h(p) = \int_0^p \frac{dp'}{\epsilon(p') + p'}. \quad (2)$$

Representing the equation of state in this way makes it possible to transform the stellar structure equations into a form that can be solved numerically more accurately and efficiently than the standard Oppenheimer-Volkoff form of the equations [1, 20].

An important feature of the enthalpy (from the perspective of the inverse stellar structure problem) is the unexpected diversity of its high pressure limit: $h_\infty \equiv \lim_{p \rightarrow \infty} h(p)$. This limit is infinite in some equations of state, while it is finite in others. For example, an equation of state of the form $\epsilon = \epsilon_0 + p$, has an enthalpy given by $h(p) = \log \sqrt{1 + 2p/\epsilon_0}$ with $h_\infty = \infty$. However the equation of state $\epsilon = \epsilon_0 e^{p/p_0} - p$, has an enthalpy given by $h(p) = p_0(1 - e^{-p/p_0})/\epsilon_0$, with $h_\infty = p_0/\epsilon_0$. This diversity in h_∞ complicates the problem of writing a robust code to find the minimum of $\chi^2(\gamma_k, h_c^i)$.

For any given equation of state, the parameters h_c^i that specify the central enthalpy of each stellar model must satisfy $h_c^i \leq h_\infty$. Since h_∞ depends on the equation of state, these conditions on h_c^i also depend on the parameters γ_k used to specify the particular equation of state: $h_c^i \leq h_\infty(\gamma_k)$. Any algorithm that explores the structure of the function $\chi^2(\gamma_k, h_c^i)$ to find its minimum, must therefore ensure that the inequalities $h_c^i \leq h_\infty(\gamma_k)$ are satisfied at every step of the process.

We assumed (implicitly) in our original implementation of the spectral approach that $h_\infty = \infty$, so it seemed unnecessary to check the conditions $h_c^i \leq h_\infty(\gamma_k)$. This error is benign whenever the initial choices for the parameters γ_k and h_c^i are close to a minimum where the conditions are satisfied. However, this limitation prevented us from exploring the structure of $\chi^2(\gamma_k, h_c^i)$ except in the immediate neighborhood of a good initial estimate. Whenever the condition $h_c^i \leq h_\infty(\gamma_k)$ was violated for some reason, our original code produced unpredictable results: sometimes generating unphysical (e.g. negative) densities, and sometimes simply crashing. This limitation therefore prevented us from using Monte Carlo

methods to explore the γ_k and h_c^i parameter space more widely, and made it impossible to determine whether any particular local minimum of $\chi^2(\gamma_k, h_c^i)$ was also its global minimum.

The minima of complicated non-linear functions like $\chi^2(\gamma_k, h_c^i)$ are generally found numerically using iterative methods. At an abstract level these methods begin with some choice of the parameters which are then refined in some way to produce an estimate that is closer to a minimum. This process is repeated until an appropriate convergence criterion is satisfied. At each step in this process the parameters must satisfy $h_c^i \leq h_\infty(\gamma_k)$, or the code which evaluates $\epsilon(h, \gamma_k)$ and $p(h, \gamma_k)$ will fail whenever h enters the range $h_\infty \leq h \leq h_c^i$. The upper limit on the range of physical enthalpies $h_\infty(\gamma_k)$ must therefore be re-evaluated at each step that changes the values of the spectral parameters γ_k . Appendix A describes in detail how the value of a good estimate $h_{\max} \leq h_\infty(\gamma_k)$ can be determined for the spectral equations of state used in our approach. The conditions $h_c^i \leq h_{\max}$ are then checked at each step of the iterative process that finds the minimum of $\chi^2(\gamma_k, h_c^i)$. If any of the h_c^i violate this condition at any step, then all the h_c^i at this step are scaled (down) so the conditions $h_c^i \leq h_{\max}$ are satisfied before proceeding. Testing and re-scaling the h_c^i (if necessary) at each step is the biggest improvement in our new more robust implementation of the spectral approach to the inverse stellar structure problem. With this change it becomes possible to use Monte Carlo methods to explore the global minimum of $\chi^2(\gamma_k, h_c^i)$.

This new improved implementation of the spectral approach to the relativistic inverse stellar structure problem has been tested using mock observational data for the masses and radii based on the 34 theoretical high-density neutron-star equations of state. These mock data sets consist of N_{stars} $[M_i, R_i]$ data pairs, with the masses uniformly spaced between $1.2M_\odot$ (a typical minimum mass for astrophysical neutron-stars) and the maximum mass M_{\max} for each theoretical equation of state. See Read, et al. [21] for descriptions of these 34 theoretical equations of state used in our tests, along with citations to the original nuclear physics papers on which they are based.

The mock data used here differ in only two minor ways from those used in our original work [1]. First, the method of extrapolating above and below the highest and lowest entries in those tabulated theoretical equations of state was changed slightly for these new tests. The new versions of our interpolation and extrapolation formulas are given in detail in Appendix B, while the old version is described in Appendix B of Ref. [1]. The second change made some (minor) corrections to some of the theoretical equation of state tables. In particular we found that some of the tabulated equations of state were non-monotonic (and therefore non-physical) at a density of about $1.67 \times 10^{12} \text{ g/cm}^3$. The effected equations of state were: APR1, APR2, APR3, APR4, ENG, H1, H2, H3, MPA1, MS1B, MS1, PCL2, PS, WFF1, WFF2, and WFF3. We corrected these problems simply by removing

the one row in each table at the density where this non-monotonicity occurred. The resulting interpolated equations of state are then monotonic. The result of these two minor changes made it possible to compute stellar models and their observational properties based on these tabulated equations of state more accurately and reliably.

In these tests of our new improved implementation of the spectral approach to the inverse stellar structure problem, we begin the calculation of the minimum of $\chi(\gamma_k, h_c^i)$ by choosing a good initial estimate for the parameters γ_k and h_c^i . We refine this initial estimate using the Levenberg-Marquardt algorithm [22] to find a local minimum of $\chi(\gamma_k, h_c^i)$. Once completed, we explore the neighborhood of this minimum by adding small random changes to each of the parameters γ_k and h_c^i . The minimum of $\chi(\gamma_k, h_c^i)$ is then recomputed using Levenberg-Marquardt with these randomized initial parameter values. This process is repeated until a minimum is found with $\chi(\gamma_k, h_c^i) < 10^{-10}$, or until 100 subsequent randomized steps fail to reduce the smallest minimum further.

The results of these tests are summarized in Table I. For each equation of state the inverse stellar structure problem has been solved by fitting N_{γ_k} different spectral parameters to mock data sets containing $N = N_{\text{stars}} = N_{\gamma_k}$ pairs of mass M_i and radius R_i data. The minimum value of the fitting function χ_N is given for each of these solutions in Table I. Two additional quantities, Δ_N^{MR} and Υ_N^{MR} are also included in Table I that measure how accurately the N parameter spectral equation of state agrees with the original used to compute the mock mass-radius observables. The function Δ_N^{MR} is defined by:

$$(\Delta_N^{MR})^2 = \frac{1}{N_{\text{eos}}} \sum_{i=1}^{N_{\text{eos}}} \left[\log \left(\frac{\epsilon(h_i, \gamma_k)}{\epsilon_i} \right) \right]^2. \quad (3)$$

The sum in Eq. (3) is over the points, $[\epsilon_i, h_i]$ from the tabulated theoretical equation of state table. Only the N_{eos} points that lie in the range $h_0 \leq h_i \leq \max h_c$ are included in this sum, where h_0 is the lower limit of the spectral domain, and $\max h_c$ is the central value of h in the maximum mass neutron star for this equation of state. The quantity Δ_N^{MR} therefore measures the average error in the spectral part of the equation of state [i.e., the part with densities above $\epsilon(h_0)$] that occur within neutron stars.¹ The best possible spectral fit to each of these theoretical neutron-star equations of state was determined in Ref. [2], and the average errors Δ_N^{EOS} of those best N_{γ_k} parameter spectral fits are given in Table II of that reference. The quantity Υ_N^{MR} measures the relative accuracy between the N parameter spectral equation of state determined by solving the inverse stellar structure

¹ We follow the convention used in Read, et al. [21] and in Lindblom and Indik [1] and choose the density $\epsilon(h_0)$ at the lower end of the spectral domain to be about half nuclear density.

problem, and the best possible spectral fit:

$$\Upsilon_N^{MR} = \frac{\Delta_N^{MR}}{\Delta_N^{EOS}}. \quad (4)$$

Except for the improvements described above, the tests performed here are identical to those performed in our original implementation of the spectral approach. The new results given in Table I are therefore directly comparable to those given in Table I of Lindblom and Indik [1]. The most obvious differences between the two tables are the values of χ_N . All of the new χ_N (except one) are less than our convergence criterion, $\chi_N < 10^{-10}$, while in contrast very few of the original χ_N were able to meet this condition. These improvements in the values of χ_N are due (mostly) to the use of Monte Carlo methods to ensure that a global rather than just a local minimum of $\chi^2(\gamma_k, h_c^i)$ is obtained.

The parameters Δ_N^{MR} in Table I that quantify the errors in the spectral equations of state are slightly larger (on average) than those obtained using our original implementation of the method. The averages of these quantities (over the 34 different theoretical equations of state) in the new tests are $\Delta_2^{MR} = 0.040$, $\Delta_3^{MR} = 0.029$, $\Delta_4^{MR} = 0.028$, $\Delta_5^{MR} = 0.024$, while the values found in the original tests were $\Delta_2^{MR} = 0.040$, $\Delta_3^{MR} = 0.029$, $\Delta_4^{MR} = 0.023$, $\Delta_5^{MR} = 0.017$. The errors in the fits with $N_{\gamma_k} = 2$ and $N_{\gamma_k} = 3$ are almost identical to those from the original tests. But the errors in the fits with $N_{\gamma_k} = 4$ and $N_{\gamma_k} = 5$ are slightly larger. The basic reason for these differences comes from the simple fact that the original method used good initial estimates of the parameters γ_k and h_c^i , followed by Levenberg-Marquardt minimization to find the nearest minimum. This local minimum was not always the global minimum of $\chi^2(\gamma_k, h_c^i)$, and in some cases (especially for larger values of N_{γ_k}) the real global minimum has somewhat larger equation of state errors than the local minimum. Despite these increases, however, the improved method still provides very good approximations to the neutron-star equation of state: i.e., average accuracy levels of just a few percent are achieved using using high precision (mock) observational data from just two or three stars.

In a few cases, the equation of state errors Δ_N^{MR} and Υ_N^{MR} in Table I are much larger than the values found using our original methods in Ref. [1]. In these cases the error quantities appear non-convergent as the number of parameters N_{γ_k} is increased. We now believe that the least squares method itself may be responsible for some of these failures. It is well known, for example, that interpolating polynomials constructed by least squares fits to data at equally spaced points are unreliable when $N^2 > 4K$, where N is the order of the polynomial fit and K the number of data points, cf §4.3.4 of Dahlquist and Björck [23]. When N exceeds this amount, the least squares method tends to produce fits that accurately pass through the K fixed data points, but oscillate wildly about the true solution between these points. This is referred to in the literature as the Runge phenomenon.

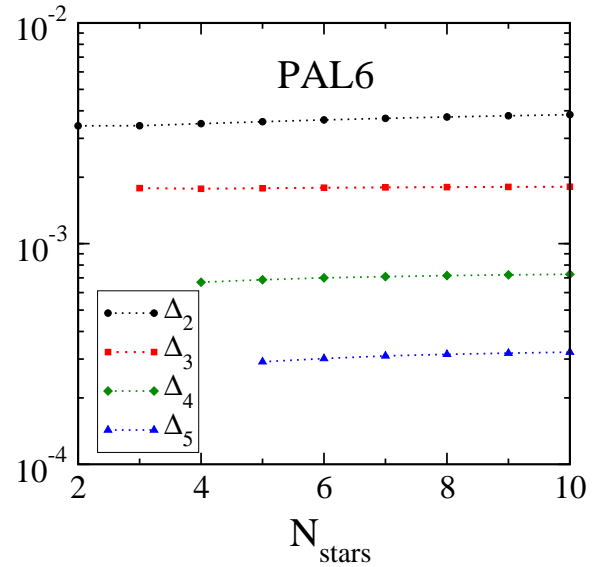


FIG. 1: Equation of state errors $\Delta_{N_{\gamma_k}}^{MR}$ as functions of the number of mass-radius data points, N_{stars} , used to fix the spectral parameters γ_k in an N_{γ_k} parameter spectral expansion. These results use mass-radius data computed with the PAL6 equation of state.

While the particular non-linear least squares minimization used in our spectral method is not strictly equivalent to polynomial interpolation, our expectation is that our method probably exhibits some form of Runge phenomenon unless appropriate restrictions are made on the number of spectral parameters, i.e., some condition of the form $N_{\gamma_k} < F(N_{\text{stars}})$.

At present we do not know an analytical expression for the function $F(N_{\text{stars}})$ that determines this stability criterion, but we can explore this question by examining the numerical convergence of our spectral equations of state. To do that we have examined in more detail the spectral solutions using mock observational data constructed from the PAL6 and the BGN1H1 equations of state. These cases represent the best (PAL6) and the worst (BGN1H1) spectral representations of the 34 equations of state used in our tests [1, 2]. Figures 1 and 2 show the dependence of the error quantities $\Delta_{N_{\gamma_k}}^{MR}$ for these cases as functions of the number of data points N_{stars} used in the solution. The results in the best case, Fig. 1, show the exponential spectral convergence that is expected in the high N limit. There are no significant changes in $\Delta_{N_{\gamma_k}}^{MR}(N_{\text{stars}})$ as N_{stars} is increased above the minimum $N_{\text{stars}} = N_{\gamma_k}$, and $\Delta_{N_{\gamma_k}}^{MR}$ decreases exponentially as N_{γ_k} increases. The worst case, Fig. 2, shows definite signs of the Runge phenomenon. The error functions $\Delta_{N_{\gamma_k}}^{MR}(N_{\text{stars}})$ for fixed N_{γ_k} in this case decrease significantly as N_{stars} increases. The BGN1H1 equation of state has a strong phase transition in the density range where the spectral methods are used, so it is not really surprising that even in the large N_{stars} limit the spectral equations of state in this case have yet

TABLE I: Accuracies of the neutron-star equations of state obtained by solving the inverse stellar structure problem using mass-radius data. Δ_N^{MR} measures the average fractional error of the equation of state obtained by fitting to N different $[M_i, R_i]$ data pairs. The parameter Υ_N^{MR} measures the ratio of Δ_N^{MR} to the errors in the optimal N -parameter spectral fit to each equation of state. The parameter χ_N measures the accuracy with which the model masses $M(h_c^i, \gamma_k)$ and radii $R(h_c^i, \gamma_k)$ produced by the approximate spectral equation of state match the exact M_i and R_i data.

EOS	Δ_2^{MR}	Δ_3^{MR}	Δ_4^{MR}	Δ_5^{MR}	Υ_2^{MR}	Υ_3^{MR}	Υ_4^{MR}	Υ_5^{MR}	χ_2	χ_3	χ_4	χ_5
PAL6	0.0034	0.0018	0.0007	0.0003	1.06	1.09	1.33	1.91	9.2×10^{-12}	4.1×10^{-11}	5.1×10^{-11}	5.2×10^{-11}
SLy	0.0107	0.0040	0.0022	0.0011	1.17	1.13	1.30	1.68	4.2×10^{-11}	5.3×10^{-11}	7.9×10^{-11}	8.3×10^{-11}
APR1	0.0746	0.0422	0.0314	0.0172	1.05	1.27	1.68	2.10	4.1×10^{-11}	2.2×10^{-11}	8.8×10^{-11}	9.4×10^{-11}
APR2	0.0313	0.0165	0.0094	0.0068	1.01	1.18	1.49	2.02	3.9×10^{-11}	8.8×10^{-11}	3.2×10^{-11}	7.2×10^{-11}
APR3	0.0266	0.0061	0.0030	0.0022	1.06	1.13	1.24	1.49	3.2×10^{-11}	2.4×10^{-11}	9.4×10^{-11}	9.8×10^{-11}
APR4	0.0258	0.0037	0.0017	0.0016	1.03	1.23	1.26	1.16	5.6×10^{-11}	3.4×10^{-11}	7.7×10^{-11}	8.1×10^{-11}
FPS	0.0047	0.0061	0.0096	0.0049	1.06	1.44	2.53	2.69	2.6×10^{-11}	3.7×10^{-11}	7.5×10^{-11}	8.3×10^{-11}
WFF1	0.0552	0.0169	0.0220	0.0158	1.04	1.59	3.19	2.41	9.6×10^{-11}	6.0×10^{-11}	6.6×10^{-11}	9.6×10^{-11}
WFF2	0.0277	0.0146	0.0084	0.0055	1.01	1.21	1.18	1.46	3.4×10^{-11}	6.4×10^{-11}	7.8×10^{-11}	9.5×10^{-11}
WFF3	0.0127	0.0147	0.0124	0.0110	1.14	1.43	2.09	1.98	3.0×10^{-11}	4.0×10^{-11}	7.1×10^{-11}	8.8×10^{-11}
BBB2	0.0332	0.0328	0.0303	0.0131	1.01	1.14	1.39	1.42	1.2×10^{-11}	4.4×10^{-11}	9.6×10^{-11}	6.8×10^{-11}
BPAL12	0.0181	0.0107	0.0068	0.0075	1.06	1.08	1.37	3.36	4.6×10^{-12}	1.3×10^{-11}	4.6×10^{-11}	5.6×10^{-11}
ENG	0.0204	0.0247	0.0201	0.0478	1.01	1.33	1.36	4.25	3.6×10^{-11}	5.6×10^{-11}	7.9×10^{-11}	9.7×10^{-11}
MPA1	0.0328	0.0040	0.0049	0.0057	1.27	1.23	1.60	2.50	7.8×10^{-11}	3.6×10^{-11}	2.3×10^{-11}	7.4×10^{-11}
MS1	0.0474	0.0157	0.0132	0.0009	1.65	2.77	3.63	2.49	5.6×10^{-11}	5.6×10^{-11}	6.6×10^{-11}	8.9×10^{-11}
MS2	0.0159	0.0044	0.0009	0.0006	1.35	1.86	2.17	3.41	1.3×10^{-15}	8.6×10^{-16}	1.3×10^{-15}	1.1×10^{-15}
MS1B	0.0305	0.0149	0.0084	0.0017	1.53	2.32	2.85	6.08	6.6×10^{-11}	6.3×10^{-11}	9.4×10^{-11}	9.3×10^{-11}
PS	0.1047	0.0779	0.1125	0.0432	1.67	2.59	3.74	2.58	6.9×10^{-11}	7.8×10^{-11}	5.7×10^{-11}	1.5×10^{-5}
GS1	0.0965	0.0604	0.0388	0.0445	1.08	1.56	1.03	1.78	5.1×10^{-12}	2.0×10^{-12}	6.1×10^{-12}	1.8×10^{-11}
GS2	0.0885	0.0888	0.1144	0.0426	1.46	2.02	2.63	1.35	3.2×10^{-11}	6.9×10^{-11}	6.7×10^{-11}	8.0×10^{-11}
BGN1H1	0.1352	0.1702	0.1356	0.1382	1.54	3.40	3.06	3.94	3.4×10^{-11}	5.2×10^{-11}	6.4×10^{-11}	9.2×10^{-11}
GNH3	0.0174	0.0183	0.0389	0.0171	1.27	1.92	4.72	2.93	8.5×10^{-12}	3.0×10^{-11}	5.7×10^{-11}	9.5×10^{-11}
H1	0.0294	0.0161	0.0127	0.0105	1.44	1.29	1.47	1.45	4.5×10^{-11}	4.1×10^{-11}	7.2×10^{-11}	9.3×10^{-11}
H2	0.0211	0.0279	0.0146	0.0221	1.19	2.01	2.12	3.22	1.7×10^{-11}	6.4×10^{-11}	4.3×10^{-11}	8.5×10^{-11}
H3	0.0139	0.0201	0.0176	0.0097	1.09	1.79	2.08	1.39	3.1×10^{-11}	3.8×10^{-11}	9.7×10^{-11}	9.9×10^{-11}
H4	0.0132	0.0259	0.0187	0.0105	1.28	2.60	2.76	1.56	8.3×10^{-11}	6.1×10^{-11}	5.7×10^{-11}	8.5×10^{-11}
H5	0.0140	0.0296	0.0118	0.0160	1.02	2.21	2.00	3.25	3.6×10^{-11}	1.0×10^{-10}	6.4×10^{-11}	8.7×10^{-11}
H6	0.0150	0.0141	0.0205	0.0157	1.09	1.03	1.57	1.38	9.1×10^{-11}	9.8×10^{-11}	7.9×10^{-11}	1.0×10^{-10}
H7	0.0134	0.0212	0.0124	0.0129	1.09	1.88	2.17	2.28	1.9×10^{-11}	8.3×10^{-11}	9.4×10^{-11}	8.5×10^{-11}
PCL2	0.0374	0.0152	0.0101	0.0250	1.35	1.16	1.04	3.06	4.8×10^{-11}	6.4×10^{-11}	2.6×10^{-11}	9.3×10^{-11}
ALF1	0.0796	0.0664	0.1040	0.0768	1.08	1.39	2.59	2.70	6.8×10^{-11}	5.6×10^{-11}	9.3×10^{-11}	9.0×10^{-11}
ALF2	0.0723	0.0598	0.0485	0.0218	1.04	1.21	1.75	1.22	5.8×10^{-11}	8.1×10^{-11}	8.6×10^{-11}	9.3×10^{-11}
ALF3	0.0404	0.0178	0.0202	0.1229	1.04	1.19	1.43	9.13	2.2×10^{-11}	5.2×10^{-11}	8.8×10^{-11}	3.1×10^{-11}
ALF4	0.0839	0.0182	0.0218	0.0394	1.18	1.35	2.19	4.15	7.6×10^{-11}	5.2×10^{-11}	9.1×10^{-11}	9.2×10^{-11}
Averages	0.0396	0.0289	0.0276	0.0239	1.22	1.65	2.14	2.77				

to enter the convergent range for the relatively small values of N_{γ_k} used in these tests. The good news is that even in this terrible case, the errors in the inferred spectral equations of state are never worse than about 20%, and it appears that results in the 5–10% range can be obtained using high quality observational data from about six stars.

We have also examined the numerical convergence of our spectral fits in more detail for several additional cases

that show significant deviations from ideal convergence: PS, GS2, ALF1, and ALF3. The sequences of error measures $\Delta_{N_{\gamma_k}}^{MR}$ given in Table I clearly appear to be non-convergent for those cases. The PS equation of state is also anomalous because it is the only case where our method fails to find a minimum of $\chi^2(\gamma_k, h_c^i)$ satisfying our convergence criterion: $\chi(\gamma_k, h_c^i) \leq 10^{-10}$. Figures 3 and 4 show the error quantities $\Delta_{N_{\gamma_k}}^{MR}$ for the PS and the

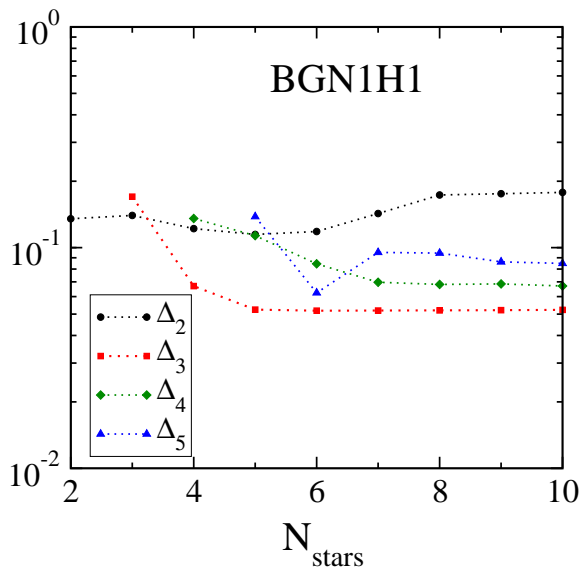


FIG. 2: Equation of state errors $\Delta_{N_{\gamma_k}}^{MR}$ as functions of the number of mass-radius data points, N_{stars} , used to fix the spectral parameters γ_k in an N_{γ_k} parameter spectral expansion. These results use mass-radius data computed with the BGN1H1 equation of state.

GS2 cases as functions of the number of data points N_{stars} used to construct the solutions. These cases both show definite signs of the Runge phenomenon: the error functions $\Delta_{N_{\gamma_k}}^{MR}(N_{\text{stars}})$ for fixed N_{γ_k} decrease significantly as N_{stars} increases. So the unexpectedly large values of $\Delta_{N_{\gamma_k}}^{MR}(N_{\text{stars}})$ seen in the $N_{\gamma_k} = N_{\text{stars}}$ solutions reported in Table I for those cases are in fact anomalous.

The other cases, ALF1 and ALF3, that we have studied in more detail are more problematic. The results for the ALF3 case are shown in Fig. 5, while those for the ALF1 case (not shown) are similar. These cases show no sign of the Runge phenomenon, yet the higher order errors Δ_5^{MR} (and Δ_4^{MR} in the ALF1 case) are much larger than the lower order errors Δ_2^{MR} and Δ_3^{MR} . We do not know exactly what is causing this problem in these cases. One possibility is that our method for finding the minimum of $\chi^2(\gamma_k, h_c^i)$ fails for some reason in these cases for larger values of N_{γ_k} . Another possibility is that these equations of state require more terms in their spectral expansions before they become truly convergent. All we can say at this point is that the spectral representations for these anomalous cases appear to be more reliable for solutions with smaller numbers of spectral parameters, i.e., the $N_{\gamma_k} = 2$ and $N_{\gamma_k} = 3$ cases, than they do for the solutions with larger numbers of parameters.

III. TIDAL DEFORMABILITY

When a star in a binary system interacts with the tidal field of its companion, it is deformed by an amount that depends on the internal structure of that star and hence

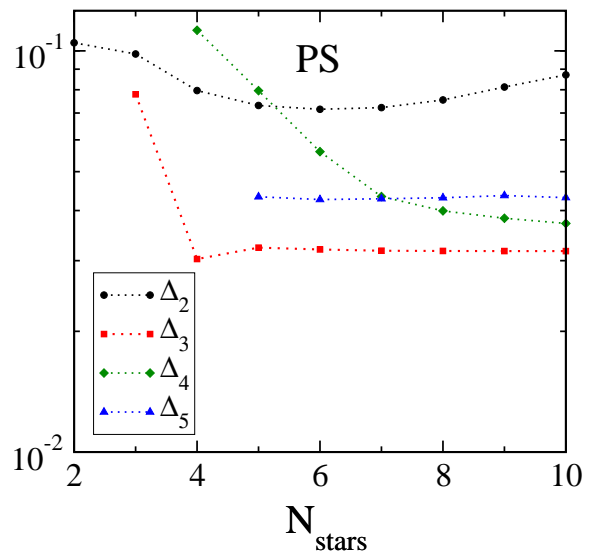


FIG. 3: Equation of state errors $\Delta_{N_{\gamma_k}}^{MR}$ as functions of the number of mass-radius data points, N_{stars} , used to fix the spectral parameters γ_k in an N_{γ_k} parameter spectral expansion. These results use mass-radius data computed with the PS equation of state.

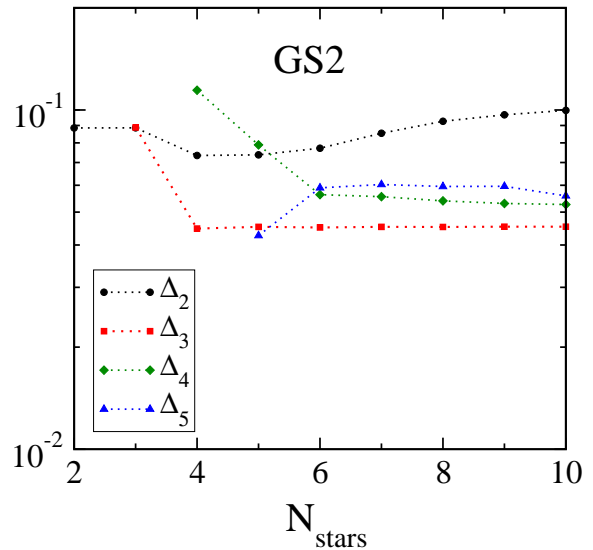


FIG. 4: Equation of state errors $\Delta_{N_{\gamma_k}}^{MR}$ as functions of the number of mass-radius data points, N_{stars} , used to fix the spectral parameters γ_k in an N_{γ_k} parameter spectral expansion. These results use mass-radius data computed with the GS2 equation of state.

the equation of state of the material from which it is made. These tidal deformations can significantly effect the phase evolutions of the last parts of the orbits of compact binary systems, so the gravitational waves emitted by such systems will contain the imprints of those tidal interactions [24–29]. Accurate observations of the gravitational waves from neutron-star binary systems will make it possible therefore to measure the tidal properties

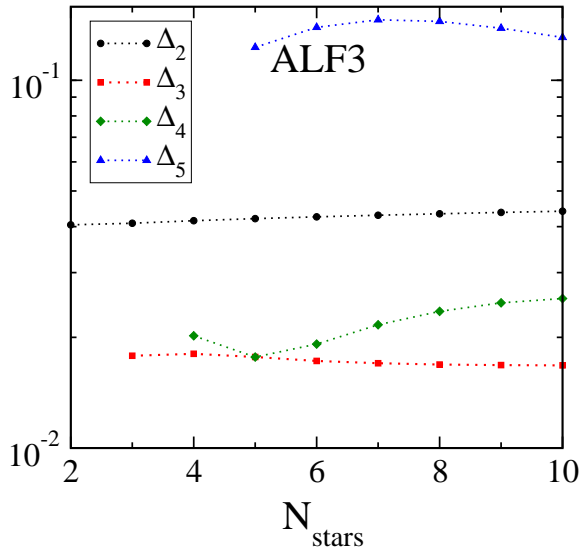


FIG. 5: Equation of state errors $\Delta_{N_{\gamma_k}}^{MR}$ as functions of the number of mass-radius data points, N_{stars} , used to fix the spectral parameters γ_k in an N_{γ_k} parameter spectral expansion. These results use mass-radius data computed with the ALF3 equation of state.

of these stars. A number of studies [3–14] have shown that the macroscopic neutron-star observable best determined by such gravitational-wave measurements are the masses M and the tidal deformabilities λ . This section explores the question, How well can the neutron-star equation of state be determined from accurate measurements of M and λ ?

The tidal deformability λ of a star is defined as the proportionality factor in the relationship between the tidal field from a star’s companion, \mathcal{E}_{ij} , and the star’s quadrupole moment, Q_{ij} , induced by that tidal interaction: $Q_{ij} = -\lambda \mathcal{E}_{ij}$. This tidal deformability λ is related to the tidal Love number k_2 by $\lambda = 2k_2 R^5/3$, and to the dimensionless tidal deformability Λ : $\Lambda = \lambda/M^5 = (2k_2/3)(R/M)^5$. Some studies [8, 12] suggest that the dimensionless tidal deformability Λ can be determined somewhat more accurately by gravitational wave observations than λ , so we use Λ in our analysis of this version of the inverse stellar structure problem. The equations needed to compute Λ (or equivalently λ or k_2) for relativistic neutron stars were first derived by Hinderer [4, 5]. Appendix C presents a more efficient way to compute $\Lambda(h_c, \gamma_k)$, as well as its derivatives with respect to the parameters γ_k and h_c for the enthalpy based representations of the parametric equations of state used in our solution of the inverse stellar structure problem: $\partial\Lambda/\partial\gamma_k$ and $\partial\Lambda/\partial h_c$. These derivatives are used by the Levenberg-Marquardt algorithm as part of our method of finding the global minimum of $\chi^2(\gamma_k, h_c^i)$.

The spectral approach to the solution of the inverse stellar structure problem described in Sec. I does not depend very strongly on which macroscopic observables are used. It is straightforward to replace the data for ob-

served masses M_i and radii R_i , with those for observed masses M_i and tidal deformabilities Λ_i . The corresponding model observables, $M(h_c^i, \gamma_k)$ and $\Lambda(h_c^i, \gamma_k)$, are evaluated using our parametrized equations of state, $\epsilon(h, \gamma_k)$ and $p(h, \gamma_k)$ with the methods described in Appendix C. The equation of state parameters γ_k (and the central enthalpy parameters h_c^i) are then fixed by minimizing the quantity $\chi(\gamma_k, h_c^i)$ that measures the differences between the observed data and the model observables:

$$\chi^2(\gamma_k, h_c^i) = \frac{1}{N_{stars}} \sum_{i=1}^{N_{stars}} \left\{ \left[\log \left(\frac{M(h_c^i, \gamma_k)}{M_i} \right) \right]^2 + \left[\log \left(\frac{\Lambda(h_c^i, \gamma_k)}{\Lambda_i} \right) \right]^2 \right\}. \quad (5)$$

We have tested the spectral approach to the relativistic inverse stellar structure problem (with the improvements described in Sec. II) using the masses and tidal deformabilities as observables. The mock observational data for the masses and tidal deformabilities used in these tests are based on the same selections of stellar models computed with the same 34 theoretical high-density neutron-star equations of state used in the tests described in Sec. II. The results of these tests are summarized in Table II. For each equation of state the inverse stellar structure problem has been solved by fitting N_{γ_k} different spectral parameters to mock data sets containing $N = N_{stars} = N_{\gamma_k}$ pairs of mass M_i and tidal deformability Λ_i data. The minimum value of the fitting function χ_N is given for each of these solutions in Table II. Two additional quantities, Δ_N^{MA} and Υ_N^{MA} are also included in Table II that measure how accurately the N parameter spectral equation of state agrees with the original used to compute the mock mass and tidal deformability observables. These equation of state error measures, Δ_N^{MA} and Υ_N^{MA} , are defined exactly as they were for the spectral equations of state computed from mass-radius data in Eqs. (3) and (4).

The results for the MA case shown in Table II are very similar, both quantitatively and qualitatively, to those from the MR case shown in Table I. All of the χ_N in Table II meet our convergence criterion $\chi_N < 10^{-10}$, except the $N_{\gamma_k} = 5$ case of the PS equation of state. This is the same exceptional case as in Table I, suggesting there is some pathology in this particular equation of state that keeps our code from finding accurate reproducible solutions to the standard stellar structure problem. Similar problems were eliminated when we corrected the non-monotonicity problems in some of the equations of state, as described in Sec. II. Unfortunately, we have not been able to identify any similar problem with the PS equation of state.

The parameters Δ_N^{MA} in Table II that quantify the errors in the spectral equations of state for the MA case are very similar to those found using using MR data in Table I. The averages of these quantities (over the 34 different theoretical equations of state) in these tests are

TABLE II: Accuracies of the neutron-star equations of state obtained by solving the inverse stellar structure problem. $\Delta_N^{M\Lambda}$ measures the average fractional error of the equation of state obtained by fitting to N different $[M_i, \Lambda_i]$ data pairs. The parameter $\Upsilon_N^{M\Lambda}$ measures the ratio of $\Delta_N^{M\Lambda}$ to the accuracy of the optimal N -parameter spectral fit to each equation of state. The parameter χ_N measures the accuracy with which the model masses $M(h_c^i, \gamma_k)$ and tidal deformability $\Lambda(h_c^i, \gamma_k)$ produced by the approximate spectral equation of state match the exact M_i and Λ_i data.

EOS	$\Delta_2^{M\Lambda}$	$\Delta_3^{M\Lambda}$	$\Delta_4^{M\Lambda}$	$\Delta_5^{M\Lambda}$	$\Upsilon_2^{M\Lambda}$	$\Upsilon_3^{M\Lambda}$	$\Upsilon_4^{M\Lambda}$	$\Upsilon_5^{M\Lambda}$	χ_2	χ_3	χ_4	χ_5
PAL6	0.0034	0.0019	0.0008	0.0003	1.05	1.19	1.53	2.20	1.1×10^{-11}	2.3×10^{-11}	3.8×10^{-11}	2.1×10^{-11}
SLy	0.0097	0.0041	0.0024	0.0013	1.07	1.16	1.41	1.94	7.5×10^{-12}	1.3×10^{-11}	6.1×10^{-12}	2.1×10^{-11}
APR1	0.0809	0.0491	0.0384	0.0199	1.14	1.48	2.06	2.43	1.7×10^{-11}	1.7×10^{-11}	1.8×10^{-11}	3.3×10^{-11}
APR2	0.0333	0.0191	0.0111	0.0082	1.08	1.37	1.75	2.41	7.2×10^{-12}	2.3×10^{-11}	1.8×10^{-11}	1.6×10^{-11}
APR3	0.0254	0.0067	0.0035	0.0026	1.01	1.23	1.44	1.75	6.8×10^{-12}	3.4×10^{-12}	7.0×10^{-12}	7.0×10^{-12}
APR4	0.0254	0.0037	0.0021	0.0018	1.02	1.25	1.56	1.33	3.8×10^{-12}	5.6×10^{-12}	1.7×10^{-11}	1.6×10^{-11}
FPS	0.0046	0.0069	0.0137	0.0076	1.03	1.63	3.60	4.18	1.1×10^{-11}	3.6×10^{-11}	7.4×10^{-12}	2.1×10^{-11}
WFF1	0.0599	0.0212	0.0340	0.0290	1.13	1.99	4.93	4.43	7.3×10^{-12}	1.3×10^{-11}	4.5×10^{-12}	2.2×10^{-11}
WFF2	0.0294	0.0172	0.0088	0.0055	1.08	1.43	1.23	1.45	3.0×10^{-12}	1.3×10^{-11}	1.2×10^{-11}	2.0×10^{-11}
WFF3	0.0141	0.0192	0.0190	0.0124	1.27	1.86	3.19	2.24	5.7×10^{-12}	7.6×10^{-12}	3.7×10^{-12}	8.0×10^{-11}
BBB2	0.0344	0.0368	0.0357	0.0143	1.04	1.28	1.64	1.55	6.8×10^{-12}	6.0×10^{-12}	1.9×10^{-11}	2.5×10^{-11}
BPAL12	0.0184	0.0118	0.0076	0.0090	1.07	1.19	1.54	4.04	9.3×10^{-12}	2.2×10^{-11}	1.3×10^{-11}	9.8×10^{-11}
ENG	0.0219	0.0243	0.0207	0.0520	1.08	1.31	1.40	4.62	4.0×10^{-12}	4.1×10^{-12}	2.2×10^{-11}	1.7×10^{-11}
MPA1	0.0301	0.0043	0.0061	0.0081	1.17	1.33	1.98	3.58	1.4×10^{-11}	1.3×10^{-11}	1.5×10^{-11}	1.6×10^{-11}
MS1	0.0465	0.0141	0.0129	0.0008	1.62	2.49	3.56	2.44	1.7×10^{-11}	1.7×10^{-11}	9.8×10^{-12}	1.9×10^{-11}
MS2	0.0155	0.0042	0.0009	0.0005	1.32	1.80	2.18	3.20	1.6×10^{-13}	4.2×10^{-13}	5.6×10^{-13}	5.7×10^{-13}
MS1B	0.0304	0.0135	0.0084	0.0014	1.52	2.10	2.82	5.08	8.0×10^{-12}	5.1×10^{-12}	1.4×10^{-11}	1.5×10^{-11}
PS	0.1044	0.0740	0.1120	0.0439	1.66	2.46	3.73	2.62	3.7×10^{-12}	1.4×10^{-11}	2.9×10^{-11}	8.0×10^{-5}
GS1	0.1018	0.0648	0.0386	0.0493	1.14	1.68	1.02	1.97	3.0×10^{-12}	1.3×10^{-12}	2.6×10^{-12}	9.5×10^{-12}
GS2	0.0909	0.0855	0.1164	0.0537	1.50	1.95	2.67	1.70	2.7×10^{-12}	4.3×10^{-12}	1.6×10^{-11}	1.9×10^{-11}
BGN1H1	0.1356	0.1652	0.1445	0.1363	1.55	3.30	3.26	3.89	1.6×10^{-11}	1.7×10^{-11}	3.5×10^{-11}	4.6×10^{-11}
GNH3	0.0182	0.0171	0.0397	0.0216	1.32	1.80	4.82	3.70	7.2×10^{-12}	5.7×10^{-12}	6.3×10^{-12}	4.3×10^{-11}
H1	0.0309	0.0154	0.0124	0.0107	1.51	1.23	1.45	1.49	2.5×10^{-11}	3.6×10^{-11}	2.1×10^{-11}	3.6×10^{-11}
H2	0.0226	0.0265	0.0153	0.0263	1.27	1.90	2.22	3.83	1.6×10^{-11}	1.1×10^{-11}	1.5×10^{-11}	1.5×10^{-11}
H3	0.0151	0.0186	0.0177	0.0118	1.18	1.66	2.09	1.70	2.0×10^{-11}	1.4×10^{-11}	1.2×10^{-11}	4.2×10^{-11}
H4	0.0119	0.0256	0.0211	0.0141	1.15	2.57	3.11	2.09	2.1×10^{-11}	1.2×10^{-11}	1.6×10^{-11}	2.1×10^{-11}
H5	0.0141	0.0293	0.0145	0.0221	1.03	2.19	2.46	4.48	7.5×10^{-12}	1.9×10^{-11}	9.7×10^{-12}	1.4×10^{-11}
H6	0.0160	0.0144	0.0204	0.0160	1.16	1.05	1.56	1.40	1.1×10^{-11}	1.2×10^{-11}	1.2×10^{-11}	1.3×10^{-11}
H7	0.0142	0.0205	0.0136	0.0170	1.16	1.83	2.38	3.00	8.7×10^{-12}	1.1×10^{-11}	2.0×10^{-11}	2.3×10^{-11}
PCL2	0.0378	0.0154	0.0103	0.0288	1.37	1.18	1.07	3.52	1.2×10^{-11}	2.4×10^{-11}	2.2×10^{-11}	4.3×10^{-11}
ALF1	0.0795	0.0704	0.1427	0.1225	1.08	1.47	3.55	4.31	3.8×10^{-11}	8.9×10^{-12}	3.8×10^{-11}	3.3×10^{-11}
ALF2	0.0725	0.0630	0.0479	0.0225	1.04	1.28	1.73	1.26	1.3×10^{-11}	1.1×10^{-11}	1.6×10^{-11}	2.3×10^{-11}
ALF3	0.0408	0.0203	0.0200	0.1566	1.05	1.36	1.42	11.64	1.1×10^{-11}	1.2×10^{-11}	2.8×10^{-11}	9.2×10^{-11}
ALF4	0.0793	0.0193	0.0213	0.0600	1.12	1.43	2.14	6.33	7.9×10^{-12}	1.3×10^{-11}	1.5×10^{-11}	3.0×10^{-11}
Averages	0.0403	0.0295	0.0304	0.0291	1.23	1.69	2.40	3.30				

$\Delta_2^{M\Lambda} = 0.040$, $\Delta_3^{M\Lambda} = 0.029$, $\Delta_4^{M\Lambda} = 0.028$, $\Delta_5^{M\Lambda} = 0.024$, while those found in the MR case were $\Delta_2^{MR} = 0.040$, $\Delta_3^{MR} = 0.030$, $\Delta_4^{MR} = 0.030$, $\Delta_5^{MR} = 0.029$. The errors in the $M\Lambda$ cases with $N_{\gamma_k} = 2$ and $N_{\gamma_k} = 3$ are almost identical to those from the analogous MR cases. But the errors in the cases with $N_{\gamma_k} = 4$ and $N_{\gamma_k} = 5$ are slightly larger. We don't know exactly why. We note that the $M\Lambda$ cases with poorest convergence properties are the same ones that show poor convergence using MR

data. This suggests that this anomalous behavior may be caused by some pathological feature of these particular equations of state, rather than some general failure of the method itself.

IV. DISCUSSION

In summary, we have improved our method of solving the relativistic inverse stellar structure problem using faithful spectral expansions of the unknown high density part of the equation of state. This method is based on minimizing a function χ that measures the differences between a given set of observables, e.g. $[M_i, R_i]$, and model values of these observables, e.g. $M(h_c^i, \gamma_k)$ and $R(h_c^i, \gamma_k)$. Our improved methods described in Sec. II are much better at finding the global minimum of this complicated non-linear function χ of the model parameters γ_k and h_c^i . The numerical tests of our improved method, described in Sec. II, consistently give much smaller values of χ than those in the tests of our original method [1]. We have also expanded our new method in Sec. III to solve the inverse stellar structure problem using the mass and tidal deformability of a star as the observables: $[M_i, \Lambda_i]$. To do this we have developed (in Appendix C) more efficient and accurate ways to evaluate the tidal deformability $\Lambda(h_c, \gamma_k)$ and its derivatives with respect to h_c and γ_k . The tests of our solution to the $[M_i, \Lambda_i]$ version of the inverse stellar structure problem show that accurate measurements of $[M_i, \Lambda_i]$ data can determine the neutron-star equation of state about as accurately as it could using the same number of accurate $[M_i, R_i]$ data. Using only two $[M_i, R_i]$ or $[M_i, \Lambda_i]$ data points, this new method can determine the high density part of the neutron-star equation of state that is present in these stars with errors (on average) of just a few percent.

Our analysis of the relativistic inverse stellar structure problem, introduced in Refs. [1, 20] and continued here in Secs. II and III, has focused on understanding some of the fundamental mathematical aspects of this problem. Is it possible to determine the neutron-star equation of state exactly from a complete knowledge of the macroscopic observable properties of these stars, i.e., does this problem have a unique solution? Can numerical methods be devised whose approximate solutions converge to the exact equation of state when a complete exact knowledge of the macroscopic observables of these stars is available? What level of numerical approximation and how many macroscopic observable data points are needed to achieve reasonable levels of accuracy for “realistic” neutron-star equations of state? While various observational and data-analysis questions related to this problem have been studied previously by a number of researchers, our studies of these fundamental questions are unique (to our knowledge).

An essential element of any practical robust solution to the inverse stellar structure problem (in our opinion) is the use of faithful parametric representations of the equation of state. These faithful representations must not exclude any physically possible equation of state, and conversely no choice of parameters may correspond to a physically impossible equation of state. To our knowledge the only faithful parametric representations of the high density equation of state discussed in the literature

are the piecewise-polytropic representations of Read, et al. [21], and our spectral representations [2] (which in general are somewhat more accurate for a given number of parameters than the piecewise-polytropes).

Özel and collaborators [15, 17, 18] and Steiner and collaborators [16, 19] have used low-order piecewise-polytropic models of the equation of state to solve the inverse stellar structure problem using presently available mass and radius measurements of neutron stars. Both groups have studied the accuracy with which the presently available $[M_i, R_i]$ data have been determined observationally. Both groups have done careful studies of the effects of these measurement errors on the accuracy with which the parameters in their high-density equation of state models are determined in this way. However, neither group has considered some of the more fundamental questions like those studied here, e.g., how accurately their solutions to the inverse stellar structure problem represent the actual neutron-star equation of state, or whether their method converges when higher-order parametric equation of state models are used in the solution.

A number of researchers have shown that tidal effects in compact binary systems can influence the gravitational waveforms they emit in an equation of state dependent way [24–29]. Flanagan and Hinderer showed that a neutron-star’s tidal deformability was the particular stellar characteristic that determines the leading-order effect on these gravitational waveforms [3]. Hinderer was the first to derive the equations that determine the tidal deformability from the structure of a relativistic stellar model [4, 5]. Hinderer and collaborators were the first to explore how the tidal deformability depends on the equation of state by evaluating it numerically for a number of theoretical neutron-star equations of state [7]. We have extended this basic formalism for evaluating the tidal deformability in this paper in two important ways. First, we derive (in Appendix C) an expression for the tidal deformability in terms of a solution to a first-order, rather than a second-order, differential equation. Our expression can therefore be evaluated numerically more accurately and efficiently. Second, we derive a set of differential equations whose solutions determine the variations of the tidal deformability with respect to the equation of state parameters. These expressions make it possible to determine these equation of state parameters from tidal deformability data more accurately and efficiently.

A number of researchers have studied how the tidal deformability of neutron stars can be measured from observations of the gravitational waves emitted by compact binary systems [6–14]. These researchers have constructed post-Newtonian [7, 13, 14], effective one body [9], and numerical relativity models [6, 8, 10–12] of the waveforms produced by these systems. They have also explored in great detail (using a variety of data-analysis methods) the expected accuracy with which the tidal deformability should be measured by the next generation of gravitational wave detectors (advanced LIGO, etc.). These researchers have shown, for example, that such measure-

ments are likely to be accurate enough to distinguish between some of the published theoretical neutron-star equations of state. None of these studies, however, has considered any of the more fundamental questions about the relativistic inverse stellar structure problem that we consider here. They have not proposed a method for determining the equation of state itself from these gravitational wave measurements, nor have they estimated how accurately it could be determined. Our study presented in Sec. III of this paper is therefore unique (to our knowledge) in its exploration of some of the fundamental questions associated with the mass and tidal deformability version of the inverse stellar structure problem.

The spectral approach to the solution of the inverse stellar structure problem introduced in Ref. [1] and improved and extended in Secs. II and III of this paper has been shown to be quite effective in determining the high-density neutron-star equation of state using high-accuracy measurements of the mass and radius (or the mass and tidal deformability) of just two or three neutron stars. However, many basic questions remain unanswered. The equations of state produced by our current implementation of the spectral approach do not converge to the exact equation of state in a few cases as the number of observational data points is increased. At the present time we do not understand the reason for this. More study of the mathematical properties of the inverse stellar structure problem is therefore needed to resolve these remaining questions.

Our studies of the inverse stellar structure problem have also assumed that the observational data were ideal. Additional research is therefore needed to explore the robustness of our approach before it can be used as a practical tool for analyzing observational data. How do the errors in the approximate spectral equations of state change when more realistic $[M_i, R_i]$ or $[M_i, \Lambda_i]$ data are used? The data used in our tests were idealized in two important ways. First, the mock $[M_i, R_i]$ or $[M_i, \Lambda_i]$ data were supplied with very high precision. Real astrophysical measurements of these quantities will have significant errors. How will measurement errors influence the accuracy of the equation of state that is constructed by these techniques? Second, the mock $[M_i, R_i]$ or $[M_i, \Lambda_i]$ data used in our tests were chosen to cover uniformly the astrophysically relevant range of neutron-star masses. Real astrophysical measurements will not be distributed in such a complete and orderly way. How will the accuracy of the implied equation of state be affected by different, presumably less ideal, data distributions? In particular, how does the accuracy of the highest-density part of the equation of state depend on the mass of the most massive neutron-star for which observational data are available?

Acknowledgments

We thank John Friedman, Tanja Hinderer, Benjamin Lackey, and Manuel Tiglio for helpful discussions concerning this research. A portion of this research was carried out during the time L.L. was a visitor at the Leonard E. Parker Center for Gravitation, Cosmology and Astrophysics, University of Wisconsin at Milwaukee. This research was supported in part by a grant from the Sherman Fairchild Foundation and by NSF grants PHY1005655 and DMS1065438.

Appendix A: Estimating $h_\infty(\gamma_k)$

The parametric representation of the equation of state used in our analysis, $\epsilon = \epsilon(h, \gamma_k)$ and $p = p(h, \gamma_k)$, is constructed from a spectral expansion of the adiabatic index $\Gamma(h)$ of the material [2]:

$$\Gamma(h) \equiv \frac{\epsilon + p}{p} \frac{dp}{d\epsilon} = \frac{\epsilon + p}{p} \frac{dp}{dh} \left(\frac{d\epsilon}{dh} \right)^{-1}, \quad (\text{A1})$$

$$= \exp \left\{ \sum_k \gamma_k \left[\log \left(\frac{h}{h_0} \right) \right]^k \right\}, \quad (\text{A2})$$

where h_0 is the lower bound on the enthalpy, $h_0 \leq h$, in the domain where the spectral expansion is to be used. This is a standard spectral expansion of the function $\log \Gamma(h)$ in which the $[\log(h/h_0)]^k$ are the spectral basis functions and the γ_k are the spectral expansion coefficients (or parameters).

The equation of state functions $p(h, \gamma_k)$ and $\epsilon(h, \gamma_k)$ are obtained from $\Gamma(h, \gamma_k)$ by integrating the system of ordinary differential equations,

$$\frac{dp}{dh} = \epsilon + p, \quad (\text{A3})$$

$$\frac{d\epsilon}{dh} = \frac{(\epsilon + p)^2}{p\Gamma(h)}, \quad (\text{A4})$$

that follow from the definitions of h and Γ in Eqs. (2) and (A1). The general solution to these equations can be reduced to quadratures:

$$p(h) = p_0 \exp \left[\int_{h_0}^h \frac{e^{h'} dh'}{\mu(h')} \right], \quad (\text{A5})$$

$$\epsilon(h) = p(h) \frac{e^h - \mu(h)}{\mu(h)}, \quad (\text{A6})$$

where $\mu(h)$ is defined as.

$$\mu(h) = \frac{p_0 e^{h_0}}{\epsilon_0 + p_0} + \int_{h_0}^h \frac{\Gamma(h') - 1}{\Gamma(h')} e^{h'} dh'. \quad (\text{A7})$$

The constants p_0 and ϵ_0 are defined by $p_0 = p(h_0)$ and $\epsilon_0 = \epsilon(h_0)$ respectively.

Equations (A5)–(A7) show that $\epsilon(h)$ and $p(h)$ are finite (for $h_0 \leq h < \infty$) unless there exists an $h = h_\infty$ where $\mu(h_\infty) = 0$. The problem of finding h_∞ is reduced therefore to the problem of finding the first zero of $\mu(h)$ above h_0 . It is not necessary for our purposes to know the exact value of h_∞ . Rather a firm estimate $h_{\max} < h_\infty$ that is beyond the range of h occurring in neutron stars is all that is needed.

Equation (A7) shows that $\mu(h_0) > 0$ and that $\mu(h)$ is monotonically increasing unless $\Gamma(h) < 1$. The first step in finding a useful estimate h_{\max} is to evaluate $\Gamma(h)$ (which can be done very efficiently) on a mesh of points covering the range $h_0 \leq h \leq h_0 e^5$. If $\Gamma(h) \geq 1$ throughout this range, then we simply set $h_{\max} = h_0 e^5$. The upper limit of this range needs to be larger than any value of h that is likely to occur within a neutron star. For the cases we have studied the value $h_0 e^5$ is a factor of 4 or 5 larger than any h we have seen in a neutron-star model, but its value could (and should) be adjusted upward as needed. If one of the mesh points, h_n , is found where $\Gamma(h_n) < 1$, then we evaluate $\mu(h)$ on a second mesh of points that covers the range $h_n \leq h \leq h_0 e^5$. If $\mu(h)$ is positive throughout this range, then we again set $h_{\max} = h_0 e^5$. If $\mu(h)$ is found to become negative somewhere in this range then we use standard numerical root finding methods to determine the location of h_∞ where $\mu(h_\infty) = 0$. In this case we set $h_{\max} = h_\infty$.

Appendix B: Interpolating and Extrapolating Equation of State Tables

This appendix describes the method for interpolating between table entries for the exact equation of states used in the tests described here. This change was motivated by our need to find the tidal deformabilities Λ of stellar models with these equations of state. The equations that determine Λ depend on the adiabatic index of the material. In our original work the equation of state below the first table entry was assumed to have uniform density, and therefore infinite adiabatic index. This choice made it difficult therefore to evaluate Λ . Consequently the method used here to extrapolate below the lowest table entries has been changed. For clarity, this appendix provides a complete description of the interpolation methods used in this paper. We assume that the exact equation of state is represented as a table of energy densities ϵ_i and corresponding pressures p_i for $i = 1, \dots, N$. For our purposes here we will convert these to an equation of state of the form $\epsilon = \epsilon(h)$ and $p = p(h)$ in the following way. We do this by assuming that the exact equation of state is obtained for values intermediate between those given in the table, $\epsilon_i \leq \epsilon \leq \epsilon_{i+1}$, by the interpolation formula:

$$\frac{p}{p_i} = \left(\frac{\epsilon}{\epsilon_i} \right)^{c_{i+1}}, \quad (\text{B1})$$

$$c_{i+1} = \frac{\log(p_{i+1}/p_i)}{\log(\epsilon_{i+1}/\epsilon_i)}. \quad (\text{B2})$$

For smaller values of the density than the lowest entry in the table, $\epsilon \leq \epsilon_1$, we assume,

$$\frac{p}{p_1} = \left(\frac{\epsilon}{\epsilon_1} \right)^{5/3}, \quad (\text{B3})$$

and for larger values of the density than the highest entry, $\epsilon \geq \epsilon_N$, we assume,

$$\frac{p}{p_N} = \left(\frac{\epsilon}{\epsilon_N} \right)^{c_N}. \quad (\text{B4})$$

The low density extrapolation given in Eq. (B3) assumes that the equation of state is that of a low temperature non-relativistic Fermi gas with adiabatic index 5/3, while the high density extrapolation given in Eq. (B4) just extends the tabulated portion of the equation of state smoothly.

Given this prescription for interpolation, it is straightforward to show that the values of the enthalpy

$$h(p) = \int_0^p \frac{dp'}{\epsilon(p') + p'}, \quad (\text{B5})$$

are given at the table entry values $h_i = h(p_i)$, by

$$h_1 = \frac{5}{2} \log \left(\frac{\epsilon_1 + p_1}{\epsilon_1} \right), \quad (\text{B6})$$

$$h_{i+1} = h_i + \frac{c_{i+1}}{c_{i+1} - 1} \log \left[\frac{\epsilon_i(\epsilon_{i+1} + p_{i+1})}{\epsilon_{i+1}(\epsilon_i + p_i)} \right]. \quad (\text{B7})$$

The pressure is determined as a function of the enthalpy, by performing the integral in Eq. (B5) to give $h(p)$, and then inverting. It is slightly more convenient to perform this inversion to give $\epsilon(h)$, from which it is straightforward to determine $p(h)$ through Eqs. (B3) and (B1):

$$\epsilon(h) = \epsilon_1 \left\{ \frac{\epsilon_1}{p_1} \left[\exp \left(\frac{2h}{5} \right) - 1 \right] \right\}^{3/2} \quad (\text{B8})$$

for $h \leq h_1$,

$$\epsilon(h) = \epsilon_i \left\{ \frac{\epsilon_i + p_i}{p_i} \exp \left[\frac{c_{i+1} - 1}{c_{i+1}} (h - h_i) \right] - \frac{\epsilon_i}{p_i} \right\}^{1/(c_{i+1} - 1)} \quad (\text{B9})$$

for $h_i \leq h \leq h_{i+1}$, and

$$\epsilon(h) = \epsilon_N \left\{ \frac{\epsilon_N + p_N}{p_N} \exp \left[\frac{c_N - 1}{c_N} (h - h_N) \right] - \frac{\epsilon_N}{p_N} \right\}^{1/(c_N - 1)} \quad (\text{B10})$$

for $h \geq h_N$.

Appendix C: Computing Λ and its Derivatives

A number of studies [3–14] have shown that the mass M and the tidal deformability λ are the neutron-star observables best measured by gravitational wave observations of neutron-star binary systems, while some studies [8, 12] suggest that the dimensionless tidal deformability $\Lambda = \lambda/M^5$ can be determined somewhat more accurately than λ itself. Hinderer [4, 5] derived the expressions for the tidal deformability λ , or equivalently the dimensionless tidal deformability Λ of a relativistic stellar model, in terms of the gravitational compactness $C = M/R$ and a quantity Y that measures the relativistic quadrupole gravitational potential induced by the tidal deformation. Using those expressions, the dimensionless tidal deformability Λ can be expressed in terms of C and Y in the following way,

$$\Lambda(C, Y) = \frac{16}{15\Xi}(1 - 2C)^2[2 + 2C(Y - 1) - Y], \quad (C1)$$

where Ξ is given by

$$\begin{aligned} \Xi(C, Y) = & 4C^3[13 - 11Y + C(3Y - 2) + 2C^2(1 + Y)] \\ & + 3(1 - 2C)^2[2 - Y + 2C(Y - 1)] \log(1 - 2C) \\ & + 2C[6 - 3Y + 3C(5Y - 8)]. \end{aligned} \quad (C2)$$

This dimensionless tidal deformability Λ is the observable we use in our study of the inverse stellar structure problem in Sec. III of this paper.

The gravitational compactness $C = M/R$ of a relativistic stellar model is computed by solving the Oppenheimer-Volkoff equations:

$$\frac{dm}{dr} = 4\pi r^2 \epsilon, \quad (C3)$$

$$\frac{dp}{dr} = -(\epsilon + p) \frac{m + 4\pi r^3 p}{r(r - 2m)}. \quad (C4)$$

The radius of the star, R , is the surface where the pressure vanishes, $p(R) = 0$, while the star's total mass, M , is $M = m(R)$.² The relativistic quadrupole gravitational potential, H , induced by the tidal interaction is determined by solving the Regge-Wheeler equation (cf Hinderer [4, 5]):

$$\begin{aligned} 0 = & \frac{d^2 H}{dr^2} + \left[\frac{2}{r} + \frac{2m + 4\pi r^3(p - \epsilon)}{r(r - 2m)} \right] \frac{dH}{dr} \\ & + \left\{ 4\pi r \left[5\epsilon + 9p + \frac{(\epsilon + p)^2}{p\Gamma} \right] \right. \\ & \left. - \frac{6}{r} - \frac{4(m + 4\pi r^3 p)^2}{r^2(r - 2m)} \right\} \frac{H}{r - 2m}. \end{aligned} \quad (C5)$$

The potential Y that appears in the expression for the tidal deformability Λ , Eq. (C1), is defined as $Y = (R/H)(dH/dr)$ evaluated at the surface of the star. Since H itself does not enter the expression for Λ , it is more efficient to transform Eq. (C5) into a form that determines only the part of the potential that is needed:

$$y = \frac{r}{H} \frac{dH}{dr}. \quad (C6)$$

The resulting first-order equation for y is given by,

$$\begin{aligned} 0 = & \frac{dy}{dr} - \frac{y^2}{r} - \frac{r + 4\pi r^3(p - \epsilon)}{r(r - 2m)} y + \frac{4(m + 4\pi r^3 p)^2}{r(r - 2m)^2} \\ & + \frac{6}{r - 2m} - \frac{4\pi r^2}{r - 2m} \left[5\epsilon + 9p + \frac{(\epsilon + p)^2}{p\Gamma} \right]. \end{aligned} \quad (C7)$$

The potential Y that appears in the expression for Λ is just the surface value of the potential y determined by solving Eq. (C7): $Y = y(R)$. The solutions to Eqs. (C3), (C4), and (C7) therefore determine the mass M , the radius R and the quadrupole deformation Y of a relativistic stellar model. The tidal deformability Λ is then determined algebraically from Eq. (C1) with $C = M/R$. This third-order system of ordinary differential equations to determine M and Λ is therefore more efficient to solve numerically than the original fourth-order system, Eqs. (C3), (C4), and (C5), derived by Hinderer [4, 5].

In our previous work on the inverse stellar structure problem [1], we found that the Oppenheimer-Volkoff equations could be solved more accurately and efficiently by transforming them into a form that determines the mass $m(h)$ and radius $r(h)$ as functions of the relativistic enthalpy h . We use this same transformation in this work to change Eq. (C7) for the relativistic quadrupole deformation $y(r)$ into an equation for $y(h)$. The resulting transformed stellar structure equations are,

$$\frac{dm}{dh} = \mathcal{M}(m, r, \epsilon, p) \equiv -\frac{4\pi r^3 \epsilon (r - 2m)}{m + 4\pi r^3 p}, \quad (C8)$$

$$\frac{dr}{dh} = \mathcal{R}(m, r, p) \equiv -\frac{r(r - 2m)}{m + 4\pi r^3 p}, \quad (C9)$$

$$\begin{aligned} \frac{dy}{dh} = & \mathcal{Y}(y, m, r, \epsilon, p, \Gamma) \equiv \frac{(r - 2m)(y + 1)y}{m + 4\pi r^3 p} + y \\ & + \frac{(m - 4\pi r^3 \epsilon)y}{m + 4\pi r^3 p} + \frac{4\pi r^3(5\epsilon + 9p) - 6r}{m + 4\pi r^3 p} \\ & + \frac{4\pi r^3(\epsilon + p)^2}{p\Gamma(m + 4\pi r^3 p)} - \frac{4(m + 4\pi r^3 p)}{r - 2m}, \end{aligned} \quad (C10)$$

where the quantities $\mathcal{M}(m, r, \epsilon, p)$, $\mathcal{R}(m, r, p)$ and $\mathcal{Y}(y, m, r, \epsilon, p, \Gamma)$ merely represent the expressions on the right sides.

The enthalpy based representation of the stellar structure Eqs. (C8)–(C10) are solved numerically by specifying conditions, $m(h_c) = r(h_c) = 0$ and $y(h_c) = 2$, at the center of the star where $h = h_c$ and then integrating these equations out to the surface of the star where

² In this paper we use geometrical units in which the gravitational constant G and the speed of light c are one: $G = c = 1$.

$h = 0$. The right sides of Eqs. (C8)–(C10), i.e., the functions $\mathcal{M}(m, r, \epsilon, p)$, $\mathcal{R}(m, r, p)$ and $\mathcal{Y}(y, m, r, \epsilon, p, \Gamma)$ are singular at the center of the star $h = h_c$. Consequently it is necessary to start any numerical integration of these equations slightly away from that singular point. The needed starting conditions can be obtained using a power series solution to the equations. The needed power series can be written in the form,³

$$r(h) = r_1(h_c - h)^{1/2} + r_3(h_c - h)^{3/2} + \mathcal{O}(h_c - h)^{5/2}, \quad (\text{C11})$$

$$m(h) = m_3(h_c - h)^{3/2} + m_5(h_c - h)^{5/2} + \mathcal{O}(h_c - h)^{7/2}, \quad (\text{C12})$$

$$y(h) = 2 + y_2(h_c - h) + \mathcal{O}(h_c - h)^2, \quad (\text{C13})$$

where r_1 , r_3 , m_3 , m_5 and y_2 are given:

$$r_1 = \left[\frac{3}{2\pi(\epsilon_c + 3p_c)} \right]^{1/2}, \quad (\text{C14})$$

$$r_3 = -\frac{r_1}{4(\epsilon_c + 3p_c)} \left[\epsilon_c - 3p_c - \frac{3(\epsilon_c + p_c)^2}{5p_c\Gamma_c} \right], \quad (\text{C15})$$

$$m_3 = \frac{4\pi}{3}\epsilon_c r_1^3, \quad (\text{C16})$$

$$m_5 = 4\pi r_1^3 \left[\frac{r_3\epsilon_c}{r_1} - \frac{(\epsilon_c + p_c)^2}{5p_c\Gamma_c} \right], \quad (\text{C17})$$

$$y_2 = -\frac{6}{7(\epsilon_c + 3p_c)} \left[\frac{\epsilon_c}{3} + 11p_c + \frac{(\epsilon_c + p_c)^2}{p_c\Gamma_c} \right]. \quad (\text{C18})$$

The quantities ϵ_c , p_c and Γ_c in these expressions are the energy density, pressure and the adiabatic index evaluated at the center of the star where $h = h_c$: $\epsilon_c = \epsilon(h_c)$, $p_c = p(h_c)$, and $\Gamma_c = \Gamma(h_c)$. We obtain the total mass $M(h_c, \gamma_k)$ and dimensionless tidal deformation $\Lambda(h_c, \gamma_k)$ by solving Eqs. (C8)–(C10) numerically starting at $h = h_c$ using an equation of state with spectral parameters γ_k . The total mass is simply the surface value $M(h_c, \gamma_k) = m(0)$ of this solution, while $\Lambda(h_c, \gamma_k)$ is determined from Eq. (C1) using the surface values $C = m(0)/r(0)$ and $Y = y(0)$.

It will be useful for our least-squares minimization problem to know how the solutions to Eqs. (C8)–(C10) change as the parameters h_c and γ_k are varied. Let η denote any one of the parameters: $\eta = \{h_c, \gamma_k\}$. We wish to derive equations for the derivatives of the solutions to these equations with respect to these parameters: $\partial m/\partial \eta$, $\partial r/\partial \eta$ and $\partial h/\partial \eta$. It is straightforward to determine the needed auxiliary equations by differentiating,

Eqs. (C8)–(C10) with respect to η :

$$\frac{d}{dh} \left(\frac{\partial m}{\partial \eta} \right) = \frac{\partial \mathcal{M}}{\partial m} \frac{\partial m}{\partial \eta} + \frac{\partial \mathcal{M}}{\partial r} \frac{\partial r}{\partial \eta} + \frac{\partial \mathcal{M}}{\partial \epsilon} \frac{\partial \epsilon}{\partial \eta} + \frac{\partial \mathcal{M}}{\partial p} \frac{\partial p}{\partial \eta}, \quad (\text{C19})$$

$$\frac{d}{dh} \left(\frac{\partial r}{\partial \eta} \right) = \frac{\partial \mathcal{R}}{\partial m} \frac{\partial m}{\partial \eta} + \frac{\partial \mathcal{R}}{\partial r} \frac{\partial r}{\partial \eta} + \frac{\partial \mathcal{R}}{\partial p} \frac{\partial p}{\partial \eta}, \quad (\text{C20})$$

$$\frac{d}{dh} \left(\frac{\partial y}{\partial \eta} \right) = \frac{\partial \mathcal{Y}}{\partial y} \frac{\partial y}{\partial \eta} + \frac{\partial \mathcal{Y}}{\partial m} \frac{\partial m}{\partial \eta} + \frac{\partial \mathcal{Y}}{\partial r} \frac{\partial r}{\partial \eta} + \frac{\partial \mathcal{Y}}{\partial \epsilon} \frac{\partial \epsilon}{\partial \eta} + \frac{\partial \mathcal{Y}}{\partial p} \frac{\partial p}{\partial \eta} + \frac{\partial \mathcal{Y}}{\partial \Gamma} \frac{\partial \Gamma}{\partial \eta}. \quad (\text{C21})$$

The various derivatives $\partial \mathcal{M}/\partial m$, etc. are determined directly from the stellar structure equations, Eqs. (C8)–(C10):

$$\frac{\partial \mathcal{M}}{\partial m} = \frac{8\pi r^3 \epsilon - \mathcal{M}}{m + 4\pi r^3 p}, \quad (\text{C22})$$

$$\frac{\partial \mathcal{M}}{\partial r} = -4\pi r^2 \frac{3p\mathcal{M} + 2\epsilon(2r - 3m)}{m + 4\pi r^3 p}, \quad (\text{C23})$$

$$\frac{\partial \mathcal{M}}{\partial p} = -\frac{4\pi r^3 \mathcal{M}}{m + 4\pi r^3 p}, \quad (\text{C24})$$

$$\frac{\partial \mathcal{M}}{\partial \epsilon} = -\frac{4\pi r^3 (r - 2m)}{m + 4\pi r^3 p}, \quad (\text{C25})$$

$$\frac{\partial \mathcal{R}}{\partial m} = \frac{2r - \mathcal{R}}{m + 4\pi r^3 p}, \quad (\text{C26})$$

$$\frac{\partial \mathcal{R}}{\partial r} = -\frac{12\pi r^2 p \mathcal{R} + 2(r - m)}{m + 4\pi r^3 p}, \quad (\text{C27})$$

$$\frac{\partial \mathcal{R}}{\partial p} = -\frac{4\pi r^3 \mathcal{R}}{m + 4\pi r^3 p}, \quad (\text{C28})$$

$$\frac{\partial \mathcal{Y}}{\partial y} = 1 + \frac{(r - 2m)2y + r - m - 4\pi r^3 \epsilon}{m + 4\pi r^3 p}, \quad (\text{C29})$$

$$\begin{aligned} \frac{\partial \mathcal{Y}}{\partial m} = & -\frac{(r - 2m)(y + 1)y}{(m + 4\pi r^3 p)^2} - \frac{(2y + 1)y}{m + 4\pi r^3 p} - \frac{4}{r - 2m} \\ & - \frac{(m - 4\pi r^3 \epsilon)y}{(m + 4\pi r^3 p)^2} - \frac{4\pi r^3 (5\epsilon + 9p) - 6r}{(m + 4\pi r^3 p)^2} \\ & - \frac{4\pi r^3 (\epsilon + p)^2}{p\Gamma(m + 4\pi r^3 p)^2} - \frac{8(m + 4\pi r^3 p)}{(r - 2m)^2}, \end{aligned} \quad (\text{C30})$$

$$\begin{aligned} \frac{\partial \mathcal{Y}}{\partial r} = & \frac{(y + 1)y}{m + 4\pi r^3 p} - \frac{12\pi r^2 p(r - 2m)(y + 1)y}{(m + 4\pi r^3 p)^2} \\ & - \frac{12\pi r^2 p(m - 4\pi r^3 \epsilon)y}{(m + 4\pi r^3 p)^2} - \frac{12\pi r^2 \epsilon y}{m + 4\pi r^3 p} \\ & + \frac{12\pi r^2 (5\epsilon + 9p) - 6}{m + 4\pi r^3 p} + \frac{12\pi r^2 (\epsilon + p)^2}{p\Gamma(m + 4\pi r^3 p)} \\ & - \frac{12\pi r^2 p[4\pi r^3 (5\epsilon + 9p) - 6r]}{(m + 4\pi r^3 p)^2} - \frac{48\pi r^2 p}{r - 2m} \\ & - \frac{48\pi^2 r^5 (\epsilon + p)^2}{\Gamma(m + 4\pi r^3 p)^2} + \frac{4(m + 4\pi r^3 p)}{(r - 2m)^2}, \end{aligned} \quad (\text{C31})$$

³ We note that the power series expansion given in Eq. (16) of Hinderer [4, 5] for $H(r)$ near $r = 0$ contains a typographical error, which has been corrected in our derivation of Eqs. (C13) and (C18).

$\eta = \gamma_k$ these derivatives can be written as

$$\frac{\partial \mathcal{Y}}{\partial \epsilon} = \frac{4\pi r^3(5-y)}{m+4\pi r^3 p} + \frac{8\pi r^3(\epsilon+p)}{p\Gamma(m+4\pi r^3 p)}, \quad (\text{C32})$$

$$\begin{aligned} \frac{\partial \mathcal{Y}}{\partial p} = & -\frac{4\pi r^3 y[(r-2m)(y+1)+m-4\pi r^3 \epsilon]}{(m+4\pi r^3 p)^2} \\ & -\frac{4\pi r^3 [4\pi r^3(5\epsilon+9p)-6r]}{(m+4\pi r^3 p)^2} + \frac{36\pi r^3}{m+4\pi r^3 p} \\ & -\frac{16\pi^2 r^6(\epsilon+p)^2}{p\Gamma(m+4\pi r^3 p)^2} + \frac{8\pi r^3(\epsilon+p)}{p\Gamma(m+4\pi r^3 p)} \\ & -\frac{4\pi r^3(\epsilon+p)^2}{p^2\Gamma(m+4\pi r^3 p)} - \frac{16\pi r^3}{r-2m}, \end{aligned} \quad (\text{C33})$$

$$\frac{\partial \mathcal{Y}}{\partial \Gamma} = -\frac{4\pi r^3(\epsilon+p)^2}{p\Gamma^2(m+4\pi r^3 p)}. \quad (\text{C34})$$

For the case when $\eta = \gamma_k$, the derivatives $\partial\epsilon/\partial\gamma_k$, $\partial p/\partial\gamma_k$ and $\partial\Gamma/\partial\gamma_k$ are determined from the equations that determine the spectral representation of the equation of state. The needed expressions are given by,

$$\frac{\partial \tilde{\mu}(h)}{\partial \gamma_k} = \int_{h_0}^h \left[\log \left(\frac{h'}{h_0} \right) \right]^k \frac{e^{h'} dh'}{\Gamma(h')}, \quad (\text{C35})$$

$$\frac{\partial p(h)}{\partial \gamma_k} = -p(h) \int_{h_0}^h \frac{\partial \tilde{\mu}(h')}{\partial \gamma_k} \frac{e^{h'} dh'}{[\tilde{\mu}(h')]^2}, \quad (\text{C36})$$

$$\frac{\partial \epsilon(h)}{\partial \gamma_k} = \frac{\partial p(h)}{\partial \gamma_k} \frac{\epsilon(h)}{p(h)} - \frac{\partial \tilde{\mu}(h)}{\partial \gamma_k} \frac{e^h p(h)}{[\tilde{\mu}(h)]^2}, \quad (\text{C37})$$

$$\frac{\partial \Gamma(h)}{\partial \gamma_k} = \left[\log \left(\frac{h}{h_0} \right) \right]^k \Gamma(h). \quad (\text{C38})$$

The integrals needed to determine these quantities can be performed accurately and efficiently using Gaussian quadrature. The equation of state does not depend on the parameter h_c , and so $\partial\epsilon/\partial h_c = \partial p/\partial h_c = \partial\Gamma/\partial h_c = 0$. Consequently the equations that determine $\partial m/\partial h_c$, $\partial r/\partial h_c$ and $\partial y/\partial h_c$ in Eqs. (C19)–(C21) are somewhat simpler than those for $\partial m/\partial\gamma_k$, $\partial r/\partial\gamma_k$ and $\partial y/\partial\gamma_k$.

The functions $\partial m/\partial\eta$, $\partial r/\partial\eta$ and $\partial y/\partial\eta$ are determined by solving Eqs. (C19)–(C21) numerically. This can be done by integrating them from the center of the star where $h = h_c$ out to the surface of the star where $h = 0$. To do this we need to impose the appropriate boundary conditions for these functions at $h = h_c$. The needed boundary conditions can be found by differentiating the power series solutions, Eqs. (C11)–(C13) with respect to the parameters η . The quantities r_1 , r_3 , m_3 , m_5 , and y_2 which appear in these power series solutions, depend on the central values of the thermodynamic quantities $\epsilon_c = \epsilon(h_c)$, $p_c = p(h_c)$, and $\Gamma_c = \Gamma(h_c)$, and through them the parameters $\eta = \{h_c, \gamma_k\}$. For the case where

$$\begin{aligned} \frac{\partial r(h)}{\partial \gamma_k} = & \left[\frac{\partial r_1}{\partial \epsilon_c} \frac{\partial \epsilon_c}{\partial \gamma_k} + \frac{\partial r_1}{\partial p_c} \frac{\partial p_c}{\partial \gamma_k} \right] (h_c - h)^{1/2} \\ & + \left[\frac{\partial r_3}{\partial \epsilon_c} \frac{\partial \epsilon_c}{\partial \gamma_k} + \frac{\partial r_3}{\partial p_c} \frac{\partial p_c}{\partial \gamma_k} + \frac{\partial r_3}{\partial \Gamma_c} \frac{\partial \Gamma_c}{\partial \gamma_k} \right] (h_c - h)^{3/2} \\ & + \mathcal{O}(h_c - h)^{5/2}, \end{aligned} \quad (\text{C39})$$

$$\begin{aligned} \frac{\partial m(h)}{\partial \gamma_k} = & \left[\frac{\partial m_3}{\partial \epsilon_c} \frac{\partial \epsilon_c}{\partial \gamma_k} + \frac{\partial m_3}{\partial p_c} \frac{\partial p_c}{\partial \gamma_k} \right] (h_c - h)^{3/2} \\ & + \left[\frac{\partial m_5}{\partial \epsilon_c} \frac{\partial \epsilon_c}{\partial \gamma_k} + \frac{\partial m_5}{\partial p_c} \frac{\partial p_c}{\partial \gamma_k} + \frac{\partial m_5}{\partial \Gamma_c} \frac{\partial \Gamma_c}{\partial \gamma_k} \right] (h_c - h)^{5/2} \\ & + \mathcal{O}(h_c - h)^{7/2}. \end{aligned} \quad (\text{C40})$$

$$\begin{aligned} \frac{\partial y(h)}{\partial \gamma_k} = & \left[\frac{\partial y_2}{\partial \epsilon_c} \frac{\partial \epsilon_c}{\partial \gamma_k} + \frac{\partial y_2}{\partial p_c} \frac{\partial p_c}{\partial \gamma_k} + \frac{\partial y_2}{\partial \Gamma_c} \frac{\partial \Gamma_c}{\partial \gamma_k} \right] (h_c - h) \\ & + \mathcal{O}(h_c - h)^2. \end{aligned} \quad (\text{C41})$$

The derivatives of r_1 , r_3 , m_3 , m_5 and y_2 with respect to the parameters ϵ_c , p_c and Γ_c which appear in Eqs. (C39)–(C41) are given by,

$$\frac{\partial r_1}{\partial \epsilon_c} = -\frac{r_1}{2(\epsilon_c + 3p_c)}, \quad (\text{C42})$$

$$\frac{\partial r_1}{\partial p_c} = 3\frac{\partial r_1}{\partial \epsilon_c}. \quad (\text{C43})$$

$$\frac{\partial r_3}{\partial \epsilon_c} = \frac{r_3}{r_1} \frac{\partial r_1}{\partial \epsilon_c} - \frac{r_1}{4(\epsilon_c + 3p_c)} \left[1 + \frac{4r_3}{r_1} - \frac{6(\epsilon_c + 3p_c)}{5p_c\Gamma_c} \right], \quad (\text{C44})$$

$$\frac{\partial r_3}{\partial p_c} = \frac{r_3}{r_1} \frac{\partial r_1}{\partial p_c} + \frac{3r_1}{4(\epsilon_c + 3p_c)} \left[1 - \frac{4r_3}{r_1} - \frac{\epsilon_c^2 - p_c^2}{5p_c^2\Gamma_c} \right], \quad (\text{C45})$$

$$\frac{\partial r_3}{\partial \Gamma_c} = -\frac{3r_1(\epsilon_c + p_c)^2}{20p_c(\epsilon_c + 3p_c)\Gamma_c^2}, \quad (\text{C46})$$

$$\frac{\partial m_3}{\partial \epsilon_c} = \frac{4\pi}{3} r_1^3 \left[1 + \frac{3\epsilon_c}{r_1} \frac{\partial r_1}{\partial \epsilon_c} \right], \quad (\text{C47})$$

$$\frac{\partial m_3}{\partial p_c} = 4\pi\epsilon_c r_1^2 \frac{\partial r_1}{\partial p_c}, \quad (\text{C48})$$

$$\begin{aligned} \frac{\partial m_5}{\partial \epsilon_c} = & 4\pi r_1^2 \left[r_3 + \frac{2\epsilon_c r_3}{r_1} \frac{\partial r_1}{\partial \epsilon_c} + \epsilon_c \frac{\partial r_3}{\partial \epsilon_c} \right] \\ & - \frac{4\pi r_1^2(\epsilon_c + p_c)}{5p_c\Gamma_c} \left[2r_1 + 3(\epsilon_c + p_c) \frac{\partial r_1}{\partial \epsilon_c} \right], \end{aligned} \quad (\text{C49})$$

$$\begin{aligned} \frac{\partial m_5}{\partial p_c} = & 4\pi\epsilon_c r_1^2 \left[\frac{2r_3}{r_1} \frac{\partial r_1}{\partial p_c} + \frac{\partial r_3}{\partial p_c} \right] \\ & + \frac{4\pi r_1^3(\epsilon_c + p_c)}{5p_c^2\Gamma_c} \left[\epsilon_c - \frac{3p_c(\epsilon_c + p_c)}{r_1} \frac{\partial r_1}{\partial p_c} \right], \end{aligned} \quad (\text{C50})$$

$$\frac{\partial m_5}{\partial \Gamma_c} = 4\pi r_1^3 \left[\frac{\epsilon_c}{r_1} \frac{\partial r_3}{\partial \Gamma_c} + \frac{(\epsilon_c + p_c)^2}{5p_c\Gamma_c^2} \right], \quad (\text{C51})$$

$$\frac{\partial y_2}{\partial \epsilon_c} = -\frac{y_2}{\epsilon_c + 3p_c} - \frac{6}{7(\epsilon_c + 3p_c)} \left[\frac{1}{3} + \frac{2(\epsilon_c + p_c)}{p_c \Gamma_c} \right] \quad (\text{C52})$$

$$\frac{\partial y_2}{\partial p_c} = -\frac{3y_2}{\epsilon_c + 3p_c} - \frac{6}{7(\epsilon_c + 3p_c)} \left[11 - \frac{\epsilon_c^2 - p_c^2}{p_c^2 \Gamma_c} \right], \quad (\text{C53})$$

$$\frac{\partial y_2}{\partial \Gamma_c} = \frac{6(\epsilon_c + p_c)^2}{7(\epsilon_c + 3p_c)p_c \Gamma_c^2}. \quad (\text{C54})$$

The values of the derivatives $\partial p_c/\partial \gamma_k$, $\partial \epsilon_c/\partial \gamma_k$ and $\partial \Gamma_c/\partial \gamma_k$ are obtained by evaluating Eqs. (C36)–(C38) at $h = h_c$.

For the case where $\eta = h_c$ the expressions for the derivatives $\partial r/\partial \eta$, $\partial m/\partial \eta$ and $\partial y/\partial \eta$ have somewhat different forms because h_c appears explicitly in the expansions in Eqs. (C11)–(C13). Differentiating these series with respect to h_c , keeping only the leading terms, gives

$$\begin{aligned} \frac{\partial r(h)}{\partial h_c} &= \frac{r_1}{2}(h_c - h)^{-1/2} \\ &+ \left[\frac{\partial r_1}{\partial \epsilon_c} \frac{\partial \epsilon_c}{\partial h_c} + \frac{\partial r_1}{\partial p_c} \frac{\partial p_c}{\partial h_c} + \frac{3r_3}{2} \right] (h_c - h)^{1/2} \\ &+ \mathcal{O}(h_c - h)^{3/2}, \end{aligned} \quad (\text{C55})$$

$$\begin{aligned} \frac{\partial m(h)}{\partial h_c} &= \frac{3m_3}{2}(h_c - h)^{1/2} \\ &+ \left[\frac{\partial m_3}{\partial \epsilon_c} \frac{\partial \epsilon_c}{\partial h_c} + \frac{\partial m_3}{\partial p_c} \frac{\partial p_c}{\partial h_c} + \frac{5m_5}{2} \right] (h_c - h)^{3/2} \\ &+ \mathcal{O}(h_c - h)^{5/2}. \end{aligned} \quad (\text{C56})$$

$$\frac{\partial y(h)}{\partial h_c} = y_2 + \mathcal{O}(h_c - h). \quad (\text{C57})$$

The derivatives of r_1 , r_3 , m_3 , and m_5 with respect to the parameters ϵ_c , p_c which appear in Eqs. (C55) and (C56) are given as before by the expressions in Eqs. (C42)–(C50), while the derivatives $\partial \epsilon_c/\partial h_c$ and $\partial p_c/\partial h_c$ are obtained directly from the definitions of the enthalpy and the adiabatic index at $h = h_c$:

$$\frac{\partial p_c}{\partial h_c} = \epsilon_c + p_c, \quad (\text{C58})$$

$$\frac{\partial \epsilon_c}{\partial h_c} = \frac{(\epsilon_c + p_c)^2}{p_c \Gamma(h_c)}. \quad (\text{C59})$$

The discussion to this point has shown how to evaluate the derivatives of M , R and Y with respect to the parameters $\eta = \{h_c, \gamma_k\}$. The quantity of primary interest in the discussion of the inverse stellar structure problem in Sec. III is the tidal deformability Λ . Its derivatives are determined by those of M , R and Y :

$$\frac{\partial \Lambda}{\partial \eta} = \frac{\partial \Lambda}{\partial C} \left(\frac{C}{M} \frac{\partial M}{\partial \eta} - \frac{C}{R} \frac{\partial R}{\partial \eta} \right) + \frac{\partial \Lambda}{\partial Y} \frac{\partial Y}{\partial \eta}. \quad (\text{C60})$$

The derivatives $\partial \Lambda/\partial C$ and $\partial \Lambda/\partial Y$ are given by,

$$\frac{\partial \Lambda}{\partial C} = \frac{2(Y-1)\Lambda}{2+2C(Y-1)-Y} - \frac{4\Lambda}{1-2C} - \frac{\Lambda}{\Xi} \frac{\partial \Xi}{\partial C}, \quad (\text{C61})$$

$$\frac{\partial \Lambda}{\partial Y} = \frac{(2C-1)\Lambda}{2+2C(Y-1)-Y} - \frac{\Lambda}{\Xi} \frac{\partial \Xi}{\partial Y}, \quad (\text{C62})$$

where

$$\begin{aligned} \frac{\partial \Xi}{\partial C} &= 4C^2[39 - 33Y + 4C(3Y - 2) + 10C^2(1 + Y)] \\ &- 12(1 - 2C)[2 - Y + 2C(Y - 1)] \log(1 - 2C) \\ &+ 6(1 - 2C)^2(Y - 1) \log(1 - 2C) \\ &- 6(1 - 2C)[2 - Y + 2C(Y - 1)] \\ &+ 6[2 - Y + 2C(5Y - 8)], \end{aligned} \quad (\text{C63})$$

$$\begin{aligned} \frac{\partial \Xi}{\partial Y} &= 4C^3(3C - 11 + 2C^2) + 2C(15C - 3) \\ &- 3(1 - 2C)^3 \log(1 - 2C). \end{aligned} \quad (\text{C64})$$

In summary, the macroscopic stellar properties M , R and Y are determined by solving the stellar structure Eqs. (C8)–(C10). The dimensionless tidal deformability Λ is then determined algebraically from them using Eq. (C1). The derivatives of these properties $\partial M/\partial \eta$, $\partial R/\partial \eta$, and $\partial Y/\partial \eta$ with respect to the parameters $\eta = \{h_c, \gamma_k\}$ are determined by solving the perturbed stellar structure Eqs. (C19)–(C21). The derivatives of the dimensionless tidal deformability $\partial \Lambda/\partial \eta$ are then determined algebraically from them using Eq. (C60).

-
- [1] L. Lindblom and N. M. Indik, Phys. Rev. D **86**, 084003 (2012).
 - [2] L. Lindblom, Phys. Rev. D **82**, 103011 (2010).
 - [3] T. Hinderer and E. Flannigan, Phys. Rev. D **77**, 021502 (2008).
 - [4] T. Hinderer, Astrophys. J. **677**, 1216 (2008).
 - [5] T. Hinderer, Astrophys. J. **697**, 964 (2009).
 - [6] J. S. Read, C. Markakis, M. Shibata, K. Uryu, J. D. E. Creighton, and J. L. Friedman, Phys. Rev. D **79**, 124033 (2009).
 - [7] T. Hinderer, B. D. Lackey, R. N. Lang, and J. S. Read, Phys. Rev. D **81**, 123016 (2010).
 - [8] B. D. Lackey, K. Kyutoku, M. Shibata, P. R. Brady, and

- J. L. Friedman, Phys. Rev. D **85**, 044061 (2012).
- [9] T. Damour, A. Nagar, and L. Villain, Phys. Rev. D **85**, 123007 (2012).
- [10] S. Bernuzzi, A. Nagar, M. Thierfelder, and B. Bruegmann, Phys. Rev. D **86**, 044030 (2012).
- [11] J. S. Read, L. Baiotti, J. D. E. Creighton, J. L. Friedman, B. Giacomazzo, K. Kyutoku, C. Markakis, L. Rezzolla, M. Shibata, and K. Taniguchi, Phys. Rev. D **88**, 044042 (2013).
- [12] B. D. Lackey, K. Kyutoku, M. Shibata, P. R. Brady, and J. L. Friedman, Phys. Rev. D (2013), arXiv:1303.6298.
- [13] W. D. Pozzo, T. G. F. Li, M. Agothos, and C. V. D. Broeck, Phys. Rev. Lett. **111**, 071101 (2013).

- [14] A. Maselli, L. Gualtieri, and V. Ferrari, *Phys. Rev. D* **88**, 104040 (2013).
- [15] F. Özel and D. Psaltis, *Phys. Rev. D* **80**, 103003 (2009).
- [16] A. W. Steiner, J. M. Lattimer, and E. F. Brown, *Astrophys. J.* **722**, 33 (2010).
- [17] T. Güver, D. Psaltis, and F. Özel, *Astrophys. J.* **747**, 76 (2012).
- [18] T. Güver and F. Özel, *Astrophys. J.* **765**, L1 (2013).
- [19] A. W. Steiner, J. M. Lattimer, and E. F. Brown, *Astrophys. J.* **765**, L5 (2013).
- [20] L. Lindblom, *Astrophys. J.* **398**, 569 (1992).
- [21] J. S. Read, B. D. Lackey, B. J. Owen, and J. L. Friedman, *Phys. Rev. D* **79**, 124032 (2009).
- [22] W. H. Press, S. A. Teukolsky, W. T. Vetterling, and B. P. Flannery, *Numerical Recipes in FORTRAN* (Cambridge University Press, Cambridge, England, 1992), 2nd ed.
- [23] G. Dahlquist and A. Björck, *Numerical Methods* (Dover Publications, 2003).
- [24] C. S. Kochanek, *Astrophys. J.* **398**, 234 (1992).
- [25] D. Lai, F. A. Rasio, and S. L. Shapiro, *Astrophys. J.* **437**, 742 (1994).
- [26] M. Vallisneri, *Phys. Rev. Lett.* **84**, 3519 (2000).
- [27] J. A. Faber, P. Grandclement, F. A. Rasio, and K. Taniguchi, *Phys. Rev. Lett.* **89**, 231102 (2002).
- [28] T. Mora and C. Will, *Phys. Rev. D* **69**, 104021 (2004).
- [29] E. Berti, S. Iyer, and C. M. Will, *Phys. Rev. D* **77**, 024019 (2008).